Soft-Switched High-Power-Factor Boost Converter

Yungtaek Jang*, Milan M. Jovanović*, Kung-Hui Fang**, and Yu-Ming Chang**

*Delta Products Corporation, Power Electronics Laboratory
P.O. Box 12173, 5101 Davis Drive, Research Triangle Park, NC 27709, USA
**Delta Electronics, Inc.
3, Tung Yuan Road, Chungli Industrial Zone, Taoyuan, Taiwan, R.O.C.

***Abstract* — A novel implementation of the high-power-factor (HPF) boost converter with active snubber is described. The snubber circuit reduces the reverse-recovery-related losses of the rectifier and also provides zero-voltage switching (ZVS) for the boost switch and zero-current switching (ZCS) for the auxiliary switch. The performance of the proposed approach was evaluated on an 80-kHz, 1.5-kW, universal-line range, HPF boost converter.**

I. INTRODUCTION

The boost converter topology has been extensively used in various ac-dc and dc-dc applications. In fact, the front end of today's ac-dc power supplies with power-factor correction (PFC) is almost exclusively implemented with boost topology. Also, the boost topology is used in numerous applications with battery-powered input to generate a high output voltage from a relatively low battery voltage.

At higher power levels, the continuous-conduction-mode (CCM) boost converter is the preferred topology for the implementation of a front end with PFC. As a result, in recent years, significant effort has been made to improve the performance of high-power boost converters. The majority of these development efforts have been focused on reducing the adverse effects of the reverse-recovery characteristic of the boost rectifier, especially for the conversion efficiency and electromagnetic compatibility (EMC).

Generally, the reduction of reverse-recovery-related losses and EMC problems require that the boost rectifier is "softly" switched off, which is achieved by controlling the turn-off rate of its current. So far, a number of soft-switched boost converters and their variations have been proposed [1]-[12]. All of them use additional components to form passive snubber or active snubber circuits that control the turn-off di/dt rate of the boost rectifier. The passive snubber approaches in [1]-[3] use only passive components such as resistors, capacitors, inductors, and rectifiers, whereas active snubber approaches employ one or more active switches.

Although passive lossless snubbers can marginally improve efficiency, their performance is not good enough to make them viable candidates for applications in high-performance PFC circuits. Generally, they suffer from increased component stresses and are not able to operate with the soft switching of the boost switch, which is detrimental in high-density applications that require increased switching frequencies.

The simultaneous reduction of reverse-recovery losses and the soft switching of the boost switch can be achieved by active snubbers. So far, a large number of active snubber circuits have been proposed [4]-[12]. The majority of them offer the soft turn off of the boost rectifier, ZVS of the boost switch, and "hard" switching of the active-snubber switch [4]-[6]. However, a number of active-snubber implementations feature soft-switching of all semiconductor components, *i.e.*, in addition to the soft turn off of the boost rectifier, the boost switch and the active-snubber switch operate with ZVS or ZCS [7]-[12].

In this paper, a novel implementation of the soft-switched boost converter with active snubber is described. The major feature of these circuits is the soft switching of all semiconductor components. Specifically, the boost rectifier is switched off with a controlled turn-off di/dt rate, the boost switch is turned on with ZVS, and the auxiliary switch in the active snubber is turned off with ZCS. As a result, switching losses are reduced, which has beneficial effects on the conversion efficiency and EMC performance.

II. SOFT-SWITCHED PFC BOOST CONVERTER

Figure 1 shows a conceptual implementation of the proposed soft-switched boost converter with ZCS of auxiliary switch S_1. After auxiliary switch S_1 is turned on, snubber inductor L_S controls the rate of change of current in the rectifier to reduce reverse-recovery-related losses in boost rectifier D. In addition, since the auxiliary-switch current cannot increase immediately because of snubber inductor L_S, the auxiliary switch turns on with ZCS. During the period when auxiliary switch S_1 is turned on, snubber inductor L_S and output capacitance C_S of boost switch S form a resonant circuit, hence the voltage across boost switch S falls to zero by resonant ringing. As a result, boost switch S turns on when its drain-to-source voltage is zero.

0-7803-8458-X/04/$20.00 ©2004 IEEE

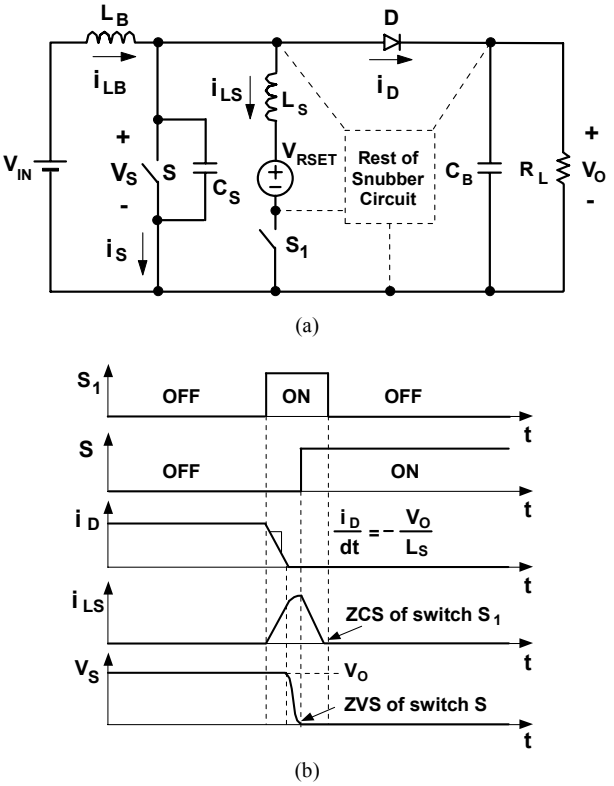

(b)

Fig. 1. Conceptual implementation of soft-switched boost converter with ZCS of snubber switch S_1: (a) conceptual circuit; (b) key waveforms during turn-on of switch S.

To reset the snubber inductor current, it is necessary to provide reset voltage V_{RSET} in the loop consisting of snubber inductor L_S and conducting switches S and S_1, as shown in Fig. 1(a). As can be seen from Fig. 1(b), auxiliary switch S_1 can achieve ZCS if it is turned off after reset voltage V_{RSET} reduces snubber-inductor current i_{LS} to zero. Reset voltage V_{RSET} can be generated either by a resonant capacitor [9] or by the winding of a low-power auxiliary transformer [7], [11], [12].

The proposed implementation of the soft-switched boost circuit is shown in Fig. 2. The circuit consists of voltage source V_{IN}, boost inductor L_B, boost switch S, boost rectifier D, energy-storage capacitor C_B, load R_L, and the active snubber circuit formed by auxiliary switch S_1, snubber inductor L_S, transformer TR, blocking diode D_1, and clamp circuit R_C-C_C-D_C.

To facilitate the explanation of the circuit operation, Fig. 3 shows a simplified circuit diagram of the circuit in Fig. 2. In the simplified circuit, energy-storage capacitor C_B and clamp capacitor C_C are modeled by voltage sources V_O and V_C, respectively, by assuming that the values of C_B and C_C are large enough so that the voltage ripples across the capacitors are small compared to their dc voltages. In addition, boost inductor L_B is modeled as constant current source I_{IN} by assuming that inductance L_B is large enough so that during a

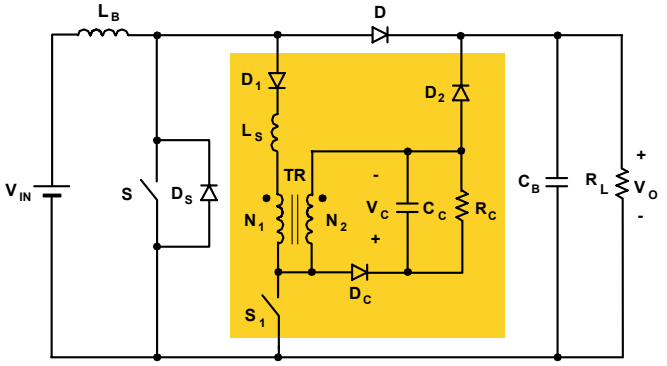

Fig. 2. Proposed soft-switched boost converter.

switching cycle the current through it does not change significantly. Also, transformer TR is modeled by magnetizing inductance L_M and an ideal transformer with turns ratio $n=N_1/N_2$. Since the leakage inductance of transformer TR is connected in series with snubber inductor L_S, it is not separately shown in Fig. 3. Finally, it is assumed that in the on state, semiconductors exhibit zero resistance, *i.e.*, they are short circuits. However, the output capacitance of the switches, as well as the junction capacitance and the reverse-recovery charge of the rectifier are not neglected in this analysis.

To further facilitate the analysis of operation, Fig. 4 shows the topological stages of the circuit in Fig. 3 during a switching cycle, whereas Fig. 5 shows its key waveforms. The reference directions of currents and voltages plotted in Fig. 5 are shown in Fig. 3.

As can be seen from the timing diagram of the drive signals for switches S_1 and S shown in Figs. 5(a) and (b), in the proposed circuit, auxiliary switch S_1 is turned on prior to the turn on of switch S. However, switch S_1 is turned off before boost switch S is turned off, *i.e.*, the proposed circuit operates with overlapping drive signals for the switches.

Prior to turn on of switch S_1 at $t=T_0$, switches S and S_1 are open and entire input current I_{IN} flows through boost rectifier

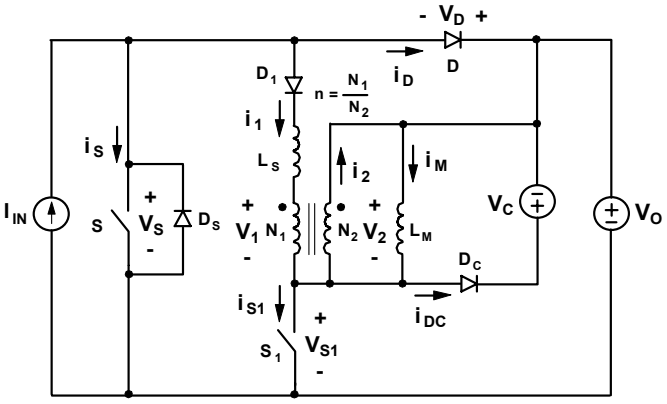

Fig. 3. Simplified circuit diagram of the proposed converter shown in Fig. 2 along with reference directions of key currents and voltages.

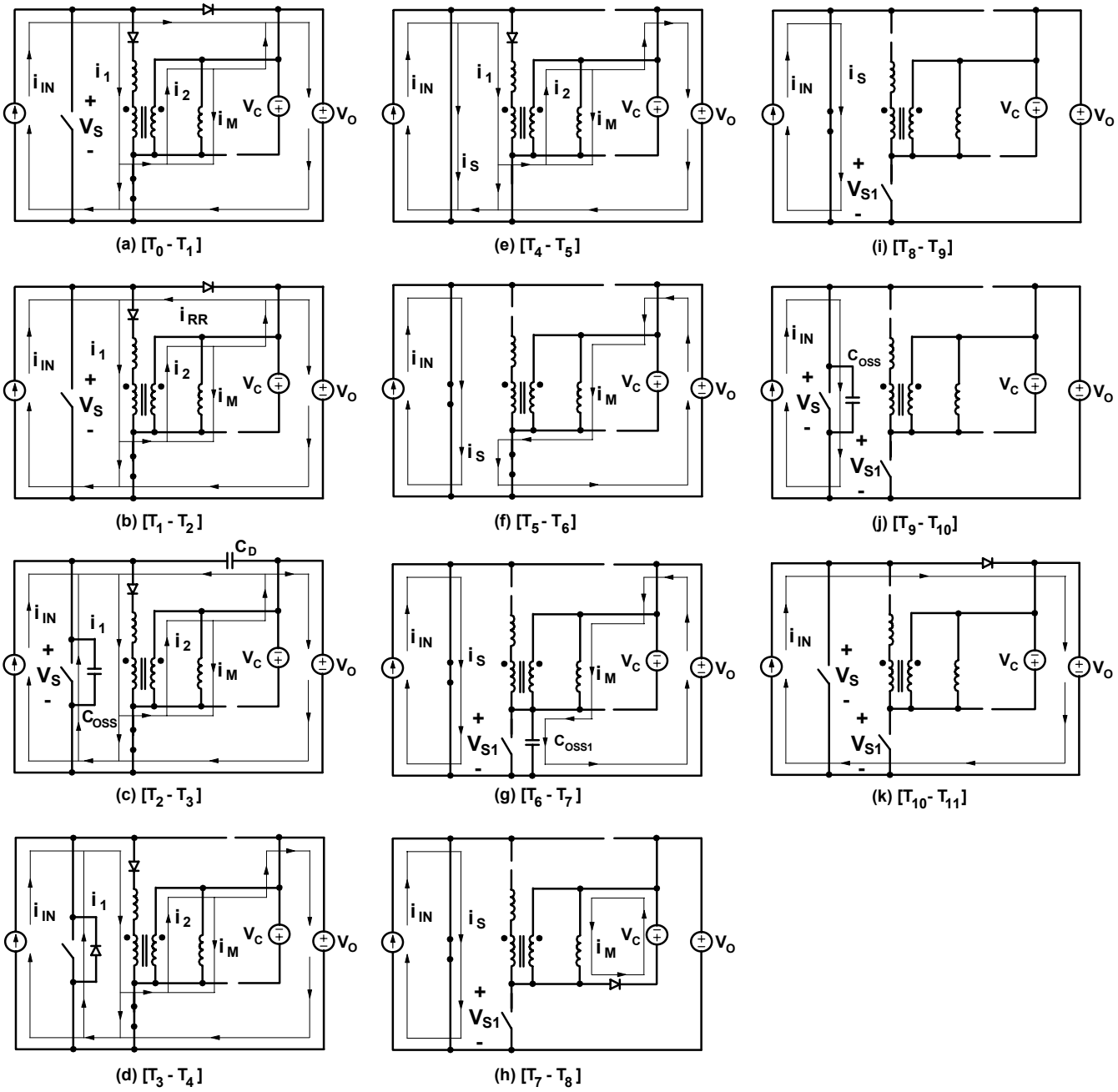

Fig. 4. Topological stages during a switching period of the proposed circuit.

D into load R_L. After switch S_1 is turned on at $t=T_0$, current i_1 starts flowing through winding N_1 of transformer TR, inducing the flow of current i_2 in winding N_2, as shown in Fig. 4(a). Because, during this stage, output voltage V_O is impressed across winding N_2, transformer winding voltages v_1 and v_2 are given by

$$v_2 = V_O \text{ and} \tag{1}$$

$$v_1 = \frac{N_1}{N_2} V_O = nV_O , \tag{2}$$

where it is required that $n=N_1/N_2<1$ for proper operation of the circuit.

Since v_1 is constant, voltage applied across snubber inductor L_S is also constant so that current i_1 increases linearly with a slope of

$$\frac{di_1}{dt} = \frac{V_O - v_1}{L_S} = \frac{V_O - nV_O}{L_S} = (1-n)\frac{V_O}{L_S} . \tag{3}$$

At the same time, magnetizing current i_M also increases with a slope given by

$$\frac{di_M}{dt} = \frac{V_O}{L_M}, \quad (4)$$

so that auxiliary switch current i_{S1} is

$$i_{S1} = i_1 - i_2 + i_M = i_1 - \frac{N_1}{N_2} i_1 + i_M = (1-n) i_1 + i_M \quad (5)$$

because $N_1 i_1 = N_2 i_2$.

As current i_1 linearly increases, boost rectifier current i_D linearly decreases at the same rate since the sum of i_1 and i_D is equal to constant input current I_{IN}, *i.e.* $i_1 + i_D = I_{IN}$. Therefore, in the proposed circuit, the turn-off rate of the boost rectifier

$$\frac{di_D}{dt} = -(1-n)\frac{V_O}{L_S} \quad (6)$$

can be controlled by proper design of turns ratio n of transformer TR and snubber inductor L_S. Typically, for today's fast-recovery rectifiers, the turn-off di_D/dt rate should be kept around 100 A/μs.

The topological stage in Fig. 4(a) ends at $t=T_1$ when boost rectifier current i_D falls to zero. Due to a stored charge in the rectifier, the rectifier current continues to flow in the negative direction, as shown in Figs. 4(b) and 5(j). Generally, for a properly selected snubber inductor L_S and turns ratio n, this reverse-recovery current is substantially reduced compared to the corresponding current in a circuit without the boost rectifier turn-off di_D/dt rate control. After the stored charge is removed from the rectifier, which occurs at $t=T_2$ in Fig. 5, the rectifier regains its voltage blocking capability and the circuit enters the topological stage shown in Fig. 4(c). During this stage, junction capacitance C_D of boost rectifier D is charged and output capacitance C_{OSS} of boost switch S discharged through a resonance between parallel connection of C_D and C_{OSS} with snubber inductor L_S. The expressions for boost-switch voltage v_S and snubber-inductor current i_1 during this resonance are

$$i_1 = I_{IN} + I_{RR(PK)} + \frac{(1-n)V_O}{Z_C}\sin(\omega_R t) \quad (7)$$

and

$$v_S = V_O - (1-n)V_O(1-\cos(\omega_R t)), \quad (8)$$

where characteristic impedance Z_C and resonant angular frequency ω_R are defined as

$$Z_C = \sqrt{\frac{L_S}{C_{OSS} + C_D}} \text{ and} \quad (9)$$

$$\omega_R = \frac{1}{\sqrt{L_S(C_{OSS} + C_D)}}. \quad (10)$$

From Eq. (8) it can be seen that to completely discharge output capacitance C_{OSS} of boost switch S and, therefore, create the condition needed for the zero-voltage turn on of switch S, it is necessary that at the end of the resonance at $t=T_3$

$$v_S(t = T_3) = V_O - (1-n)V_O(1-\cos\pi) = 0, \quad (11)$$

which limits maximum turns ratio n_{MAX} of transformer TR to

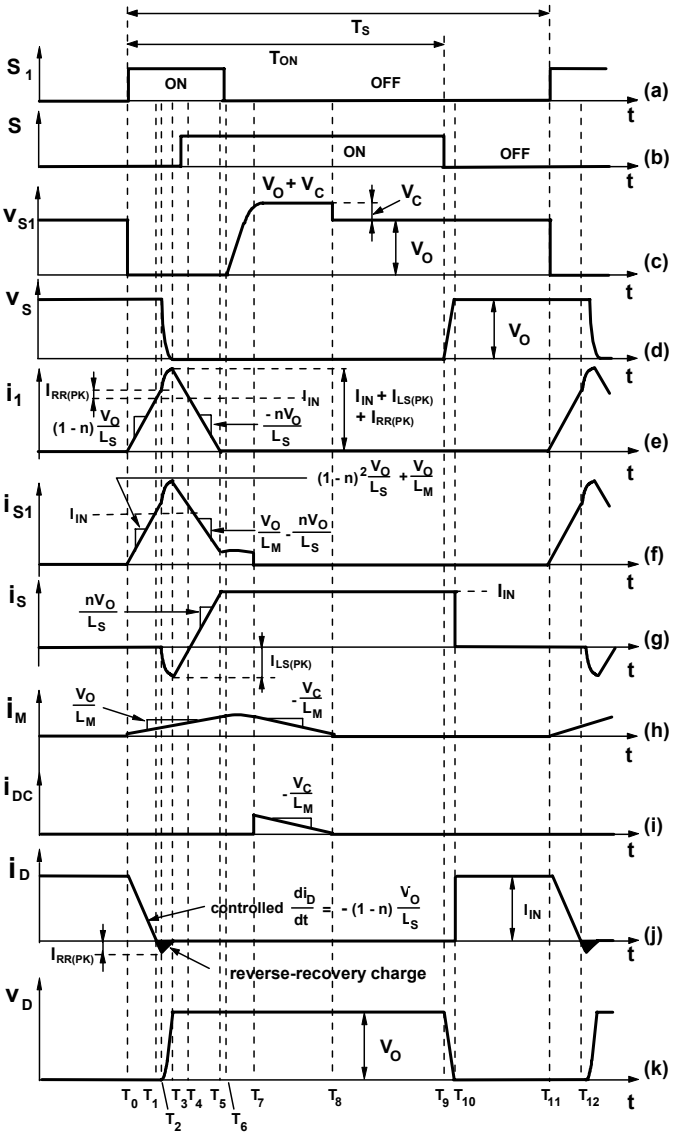

Fig. 5. Key waveforms of the proposed converter.

$$n_{MAX} = 0.5. \quad (12)$$

If a turns ratio of $n<0.5$ is selected, output capacitance C_{OSS} of boost switch S can be always discharged to zero regardless of the load and line conditions. Once the capacitance is fully discharge at $t=T_3$, current i_1 continues to flow through the antiparallel diode of boost switch S, as shown in Fig. 4(d). Because during this topological stage voltage v_1 is impressed in the negative direction across snubber inductor L_S, current i_1 starts linearly decreasing at the rate given by

$$\frac{di_1}{dt} = -\frac{nV_O}{L_S}, \quad (13)$$

as illustrated in Fig. 5(e). As a result, auxiliary-switch current i_{S1} also starts linearly decreasing, whereas boot-switch

current i_S starts linearly increasing from a negative peak, as shown in Figs. 5(f) and (g). To achieve ZVS of boost switch S, it is necessary to turn on boost switch S before its current becomes positive at $t=T_4$, *i.e.*, while current i_S is flowing through the antiparallel diode of switch S.

With boost switch S turned on before $t=T_4$, boost-switch current i_S continues to flow through closed switch S after it becomes positive at $t=T_4$, as shown in Figs. 4(e) and 5(g). In this topological stage, current i_1 continues to decrease linearly toward zero, while boost-switch current i_S continues to linearly increase at the same rate. When current i_1 becomes zero at $t=T_5$, boost-switch current i_S reaches I_{IN} so that the entire input current I_{IN} flows through boost switch S, as shown in Fig. 4(f). At the same time, auxiliary switch S_1 only carries a magnetizing current. If the magnetizing inductance of the transformer is made high, the magnetizing current can be minimized, *i.e.*, it can be made much smaller than input current I_{IN} so that auxiliary switch S_1 can be turned off with virtually zero current.

When auxiliary switch S_1 is turned off with near ZCS at $t=T_6$, magnetizing current i_M begins charging output capacitance C_{OSS1} of auxiliary switch S_1, as shown in Fig. 4(g). When voltage v_{S1} across auxiliary switch S_1 reaches clamp voltage V_O+V_C, where V_C is the voltage across clamp capacitor C_C, magnetizing current i_M is commutated into voltage source V_C, which models the clamp circuit. As shown in Fig. 4(h), during this stage, negative voltage V_C resets the magnetizing current with a rate

$$\frac{di_M}{dt} = -\frac{V_C}{L_M} \qquad (14)$$

until magnetizing current i_M becomes zero at $t=T_8$.

After transformer TR is reset at $t=T_8$, the circuit stays in the topological stage shown in Fig. 4(i) until boost switch S is opened at $t=T_9$ and the input current is commutated from switch S to its output capacitance C_{OSS}, as shown in Fig. 4(j). Due to C_{OSS} charging with constant current I_{IN}, voltage v_S is increasing linearly until it reaches V_O at $t=T_{10}$ and input current I_{IN} is instantaneously commutated to boost rectifier, as shown in Fig. 4(k). The circuit stays in the topological stage in Fig. 4(k) until $t=T_{11}$ when auxiliary switch S_1 is turned on again.

It should be noted that in the previous analysis the junction capacitance of diode D_1 was neglected since it has no significant effect on the operation of the circuit. In fact, this capacitance plays a role only during a brief interval after current i_1 reaches zero at $T=t_5$. Specifically, after $T=t_5$, the junction capacitance of diode D_1 and snubber inductor L_S resonate creating a small negative current i_1 that makes auxiliary-switch current i_{S1} flow in the negative direction through the antiparallel diode of switch S_1. Due to the conduction of its antiparallel diode, auxiliary switch voltage v_{S1} does not immediately start to increase after switch S_1 is turned off at $T=t_6$, *i.e.*, shortly after i_{S1} falls to zero. Instead, the rise of v_{S1} is briefly delayed until the current through the antiparallel diode resonates back to zero. This delay has no tangible effect on the operation or the performance of the circuit.

In summary, the major feature of the proposed circuit is the soft-switching of all semiconductor devices. Specifically, boost switch S is turned on with ZVS, auxiliary switch S_1 is turned off with ZCS, and boost diode D is turned off with a controlled turn-off di_D/dt rate. As a result, the turn-on switching loss of the boost switch, the turn-off switching loss of the auxiliary switch, and reverse-recovery-related losses of the boost rectifier are eliminated, which minimizes the overall switching losses and, therefore, maximizes the conversion efficiency. In addition, soft-switching has a beneficial effect on EMI that may result in a smaller volume input filter.

Due to ZVS of the boost switch, the most suitable implementation of the circuit in Fig. 2 is with the boost switch consisting of a MOSFET (Metal Oxide Semiconductor Field Effect Transistor) device or a parallel combination of MOSFETs. Similarly, due to the ZCS of the auxiliary switch, the circuit in Fig. 2 is suitable for an IGBT (Insulated Gate Bipolar Transistor) auxiliary switch. However, the circuit can be also implemented with a MOSFET auxiliary switch without a significant performance penalty. Moreover, even an implementation with an IGBT boost switch is possible provided that a turn-off snubber capacitor is connected across the IGBT boost switch to reduce the turn-off loss due to the IGBT's current-tail effect. In this case, an IGBT with a co-packaged antiparallel diode or an external diode must be used.

In the proposed circuit, the voltage and current stress on boost switch S and boost rectifier D are identical to the corresponding stress in the conventional boost converter without a snubber. However, the voltage stress of the auxiliary switch is

$$v_{S1(MAX)} = V_O + V_C, \qquad (15)$$

while the current stress, neglecting residual reverse-recovery current $I_{RR(PK)}$ and magnetizing current i_M, is

$$i_{S1(MAX)} \cong (1-n)\left[I_{IN} + \frac{(1-n)V_O}{Z_C}\right], \qquad (16)$$

as illustrated in Figs. 5(c) and (f).

According to Eq. (15), the voltage stress of auxiliary switch S_1 can be controlled by the selection of clamp voltage V_C. Generally, this voltage is determined by the energy stored in magnetizing inductance L_M during the conduction period of auxiliary switch S_1 and the value of clamp resistor R_C. If capacitor C_C is selected large enough so the ripple of voltage across it is much smaller than the average value, voltage V_C can be calculated from

$$\frac{1}{2}L_M\left(\frac{V_O}{L_M}D_{S1}T_S\right)^2 f_S = \frac{V_C^2}{R_C}, \qquad (17)$$

where D_{S1} is the duty cycle of auxiliary switch S_1, T_S is the switching period, and $f_S=1/T_S$ is the switching frequency.

Since, from Eq. (17),

$$V_C = \sqrt{\frac{R_C}{2f_S L_M}}\left(D_{S1} V_O\right), \qquad (18)$$

the best way to minimize V_C is to maximize magnetizing inductance L_M so that the power loss of the clamp circuit, *i.e.*, the power dissipation of R_C, is also minimized. Typically, for a properly designed transformer TR, the clamp-circuit loss is negligible compared to the output power so it virtually does not affect the conversion efficiency.

The snubber inductor L_S is determined from the desired turn-off rate of the boost rectifier current defined in Eq. (6), *i.e.*,

$$L_S = \frac{(1-n)V_O}{di_D/dt}. \qquad (19)$$

As can be seen from Eq. (19), to minimize the value of snubber inductor L_S, it is desirable to maximize turns ratio n of the transformer. Since n_{MAX}=0.5, the turns ratio of the transformer should not be much less than 0.5. Typically, the values of n that are in the 0.3-0.5 range are optimal. Assuming that V_O=400 V, n=0.5, and di_D/dt=100 A/μs, the inductance value of snubber inductor L_S is 2 μH.

III. Experimental Results

The performance of the proposed boost converter with active snubber was evaluated on a 1.5 kW (375 V/3.95 A), 80 kHz, PFC circuit operating at universal-line range (85 - 264 V_{AC}).

Since the drain voltage of boost switch S is clamped to bulk capacitor C_B, the peak voltage stress on boost switch S is approximately 380 V. The peak current stress on switch S, which occurs at full load and low line, is approximately 27.7 A. Therefore, three IRFP460LC MOSFETs (V_{DSS} = 500 V, I_{D25} = 20 A, R_{DS} = 0.27 Ω) from IRF were used for boost switch S. A high speed HGTG12N60A4 IGBT (V_{RRM} = 600 V, I_F = 23 A) from Fairchild was used as auxiliary switch S_1 since its maximum drain voltage is $V_{S1(MAX)} = V_O+V_C$ = 380+60 = 440 V, as described in Eq. (15). To clamp the voltage across switch S_1, clamp diode D_C (BYM26C), clamp capacitor C_C (0.1 μF, 100 V), and clamp resistor R_C (5.1 kΩ, 2W) were used as shown in Fig. 2. The calculated maximum power dissipation of clamp resistor R_C is approximately 0.7 W.

Since boost diode D should block the bulk voltage and conduct the peak input current, an RHRP3060 diode (V_{RRM} = 600 V, I_{FAVM} = 30 A) from Fairchild was used. Two RHRP1560 diodes (V_{RRM} = 600 V, I_{FAVM} = 15 A) were used as diode D_1 and diode D_2.

To obtain the desired inductance of boost inductor L_B, the boost inductor was built using two glued toroidal powder cores (77071, μ=60) from Magnetics and 72 turns of magnet wire (AWG #18).

An external snubber inductor was connected in series with winding N_1 of transformer TR, as shown in Fig. 2. To obtain required snubber inductance that is approximately 1.7 μH at full load, the external snubber inductor was built using a toroidal powder core (MS90060, μ=60) from Arnold and 6 turns of magnet wire (AWG #16).

Transformer TR was built using a toroidal ferrite core (A07 T25x15x13C), 10 turns of magnet wire (AWG# 18) for winding N_1, and 40 turns of magnet wire (AWG# 21) for winding N_2. Magnetizing inductance L_M measured across winding N_2 of transformer TR is approximately 12 mH. The leakage inductance measured across winding N_1 of transformer TR is approximately 0.3 μH.

Two high voltage aluminum capacitors (470 μF, 450 VDC) were used for bulk capacitor C_B to meet the hold-up time requirement.

Figure 6 shows the oscillograms of key waveforms of the experimental converter when it delivers full power from the low line. As can be seen from the corresponding waveforms in Fig. 5, there is good agreement between the experimental

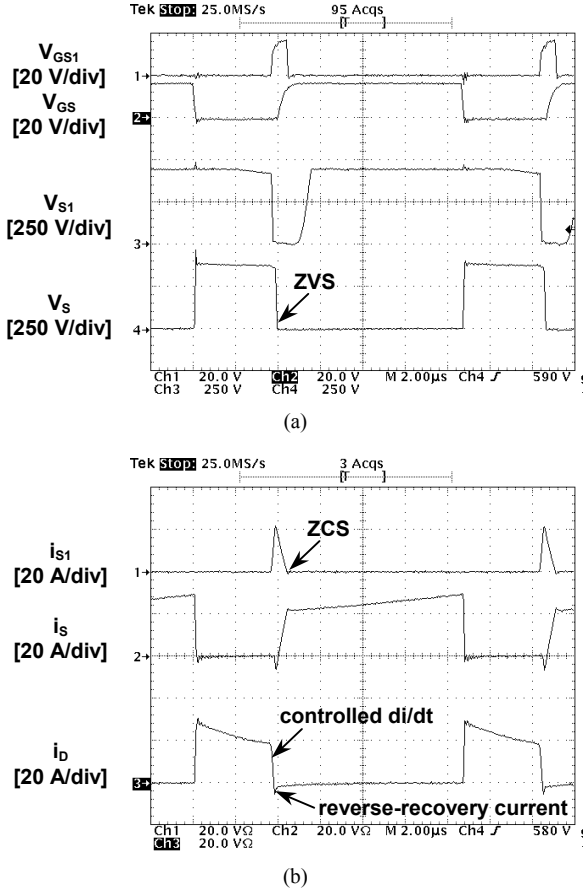

Fig. 6. Measured key waveforms of experimental converter at P_O = 1500 W and V_{IN} = 85 V_{AC}. Time base: 2 μs/div.

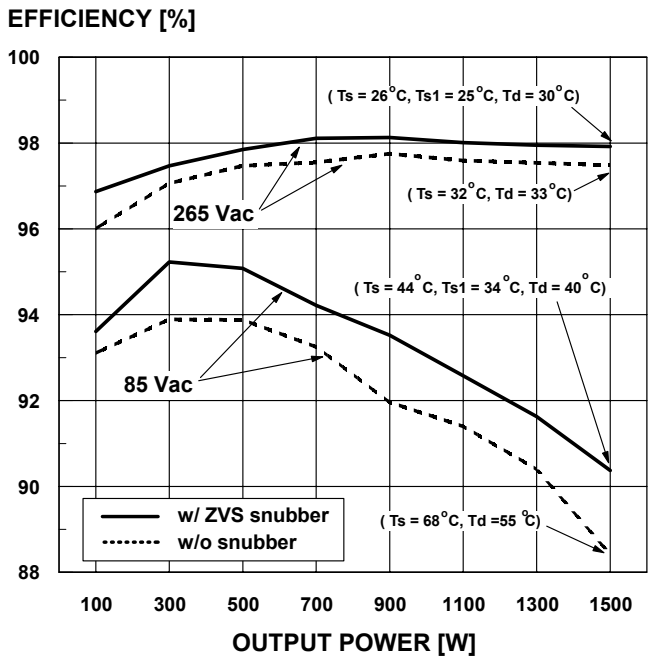

Fig. 7. Measured efficiencies of the 80-kHz, 1.5-kW experimental converter with (dashed lines) hard switching and (solid lines) soft switching at V_{IN} = 85 V_{AC} and 265 V_{AC} as functions of the output power.

and theoretical waveforms.

Figure 7 shows the measured efficiencies of the experimental converter with and without the active snubber at the minimum and the maximum line voltages as functions of the output power. The active snubber improves the conversion efficiency for both line voltages. Nevertheless, the efficiency improvement is more pronounced at the minimum line and higher power levels where the reverse-recovery losses are greater. Specifically, at the maximum line (265 V_{AC}), the efficiency improvement at 1.5 kW is 0.5%. However, at the minimum line and P_O=1.5 kW, the active snubber improves the efficiency by approximately 2%, which translates into approximately 20% reduction of all losses. Furthermore, at the same power levels, the temperatures of the semiconductor components in the implementation with the active snubber are significantly lower than those in the implementation without the snubber.

Finally, since the boost switch and auxiliary switch operate with soft switching, the rectifier reduces switching losses and thereby improves the spectral performance of the rectifier for less EMI.

IV. SUMMARY

A novel implementation of the PFC boost converter with an active snubber that can achieve soft-switching of all semiconductor devices in the power stage has been introduced. By using an active snubber that consists of an auxiliary switch, a snubber inductor, and a reset circuit, boost switch S is turned on with ZVS, auxiliary switch S_1 is turned off with ZCS, and boost diode D is turned off softly using a controlled di_D/dt rate. As a result, the turn-on switching losses in the boost switch, the turn-off switching loss in the auxiliary switch, and reverse-recovery-related losses in the boost diode are eliminated, which maximizes the conversion efficiency. The performance of the proposed converter was verified on an 80-kHz, 1.5-kW prototype circuit that was designed to operate from a universal ac-line input. The proposed technique improves the efficiency by approximately 2% at full load and low line.

REFERENCES

[1] K. M. Smith, K. M. Smedley, "Engineering design of lossless passive soft switching methods for PWM converters," *IEEE Applied Power Electronics Conf. (APEC) Proc.,* pp. 1055 – 1061, 1998.

[2] S. Ben-Yakov, G. Ivensky, "Passive lossless snubbers for high frequency PWM converters," *IEEE Applied Power Electronics Conf. (APEC) Professional Education Seminar Book,* Seminar 12, 1999.

[3] C. J. Tseng, C. L. Chen, "Passive lossless snubbers for dc/dc converters," *IEEE Applied Power Electronics Conf. (APEC) Proc.,* pp. 1049 – 1054, 1998.

[4] R. Streit, D. Tollik, "High efficiency telecom rectifier using a novel soft-switched boost-based input current shaper," *International Telecommunication Energy Conf. (INTELEC) Proc*., pp. 720-726, Oct. 1991.

[5] G. Hua, C.S. Leu, F.C. Lee, "Novel zero-voltage-transition PWM converters," *IEEE Power Electronics Specialists' Conf. (PESC) Rec*., pp. 55-61, June 1992.

[6] J.-H. Kim, D.Y. Lee, H.S. Choi, B.H. Cho, "High performance boost PFP (power factor pre-regulator) with an improved ZVT (Zero Voltage Transition) converter," IEEE *Applied Power Electronics (APEC) Conf. Proc.*, pp. 337-342, 2001.

[7] D.C. Martins, F.J.M. de Seixas, J.A. Brilhante, I. Barbi, "A family of dc-to-dc PWM converters using a new ZVS commutation cell," *IEEE Power Electronics Specialists' Conf. (PESC) Rec*., pp. 524 - 530, 1993.

[8] C.A. Canesin, I. Barbi, "Comparison of experimental loses among six different topologies for a 1.6kW boost converter, using IGBT's," IEEE *Power Electronics Specialists' Conf. (PESC) Rec*., pp. 1265-1271, 1995.

[9] G. Moschopoulos, P. Jain, G. Joós, "A novel zero-voltage switched PWM boost converter," IEEE *Power Electronics Specialists' Conf. (PESC) Rec*., pp. 694-700, 1995.

[10] J. Bassett, "New, zero voltage switching, high frequency boost converter topology for power factor correction," *International Telecommunication Energy Conf. (INTELEC) Proc*., pp. 813-820, Oct. 1995.

[11] R.L. Lin, Y. Zhao, F.C. Lee, "Improved soft-switching ZVT converters with active snubber," *IEEE Applied Power Electronics (APEC) Conf. Proc.*, pp. 1063 - 1069, 1998.

[12] H. Matsuo, F. Kurokawa, T. Oshikata, and Y. Yamawaki, "Analysis of dynamic characteristics for the partially resonant active filter with the DSP," *International Telecommunication Energy Conf. (INTELEC) Proc*., pp. 81-88, Oct. 2001.